Landscape Ecology (2006) 21:195–211
DOI 10.1007/s10980-005-0145-6

Research article

Simulating spatial nitrogen dynamics in a forested reference watershed, Hubbard Brook Watershed 6, New Hampshire, USA

Bongghi Hong*, Dennis P. Swaney and David A. Weinstein
*Boyce Thompson Institute for Plant Research, Cornell University, Tower Road, Ithaca, NY 14850, USA; *Author for correspondence: 106 Illick Hall, SUNY-ESF, 1 Forestry Drive, Syracuse, NY 13210, USA (e-mail: bohong@mailbox.syr.edu)*

Received 7 June 2004; accepted in revised form 23 June 2005

Key words: Forest biogeochemistry, Nitrogen cycling, Spatial modeling, Watershed dynamics

Abstract

We demonstrate that available information on spatial heterogeneity in biotic, topographic, and climatic variables within a forested watershed, Hubbard Brook Experimental Forest (HBEF) Watershed 6, New Hampshire, USA, was sufficient to reproduce the observed elevational pattern in stream NO_3 concentration during the 1982–1992 period. Five gridded maps (N mineralization factor, N uptake factor, precipitation, elevation, and soil depth factor) were created from spatial datasets and successively added to the spatially explicit model SINIC-S as spatially varying input parameters. Adding more spatial information generally improved model predictions, with the exception of the soil depth factor. Ninety percent of the variation in the observed stream NO_3 concentration was explained by the combination of the spatial variation of the N mineralization and N uptake factors. Simulated streamflow NO_3 flux at the outlet point was improved slightly by introducing spatial variability in the model parameters. The model exhibited substantial cell-to-cell variation in soil N dynamics and NO_3 loss within the watershed during the simulation period. The simulation results suggest that the spatial distributions of forest floor organic matter and standing biomass are most responsible for creating the elevational pattern in stream NO_3 concentration within this watershed.

Introduction

Significant elevational variations in stream NO_3 concentration have been reported within forested watersheds, but reported patterns are complex and inconsistent across watersheds. For example, Johnson et al. (2000a) measured stream NO_3 concentrations at six points (544, 602, 663, 701, 733, and 751 m) along the elevational gradient in the first-order stream of Watershed 6 (W6) at Hubbard Brook Experimental Forest (HBEF), New Hampshire, between 1982 and 1992, and reported that the highest concentration occurred at the middle position (701 m), whereas Lawrence et al. (2000) reported that from 1991 to 1994, the NO_3 concentration of the first-order stream at Winnisook watershed in the Catskill Mountains, New York, showed a decreasing trend with elevation.

The elevational variation in stream NO_3 concentration may be controlled by both in-stream and upland nitrogen processes. With increasing distance downstream traveled by the stream NO_3 molecule, there is a greater chance to be held by transient storages like the hyporheic zone (Hinkle et al. 2001) and removed from the water via

transformations and biotic N demand (Bernhardt et al. 2002). Although in-stream processes have been shown to play an important role in some watersheds (Hinkle et al. 2001; Wickham et al. 2003), stream biological processes and transient storages within HBEF were not sufficient in explaining the spatial variation in stream NO_3 concentration (Bernhardt et al. 2002; Hall et al. 2002).

Studies conducted at Hubbard Brook (Bohlen et al. 2001) and other watersheds (Williard et al. 1997; Christ et al. 2002) showed that the variation in streamflow NO_3 flux may be closely linked to the soil N dynamics in the drainage area. The streamflow N flux at any point reflects the integrated pattern of soil N dynamics in the watershed above that point. Thus, accounting for spatial variability of the soil N processes within the watershed should lead to more accurate prediction of variation in stream N concentrations along the elevational gradient. Estimating the spatial variability of soil N dynamics is difficult, however, because soil N dynamics have been shown to vary substantially even at small scales (Manderscheid and Matzner 1995; Brierley et al. 2001; Laverman et al. 2000) and measurements of soil N dynamics to account for the spatial heterogeneity are often prohibitively expensive (Clay et al. 1997; Johnson et al. 2000b). Attempts to relate more available information, such as topography (Johnson et al. 2000b; Christ et al. 2002) and species composition (Lovett et al. 2000), to soil N dynamics have met with only partial success.

In this study, we present a modeling approach to identify the biotic, topographic, and climatic variables whose spatial variation contributed to the measured elevational pattern of stream NO_3 concentration at HBEF W6. We use a grid layout developed for this small (13.2 ha) forested watershed in 1965, consisting of 208 25×25 m cells (Figure 1). Although HBEF has one of the richest datasets in the world, only limited spatially referenced data are available (http://www.hubbardbrook.org), including forest inventory, forest floor organic mass, elevation, till depth, and precipitation measured at three different stations around W6.

The spatially explicit model, SINIC-S, simulates the spatial patterns of nitrogen dynamics within a watershed using several gridded maps created

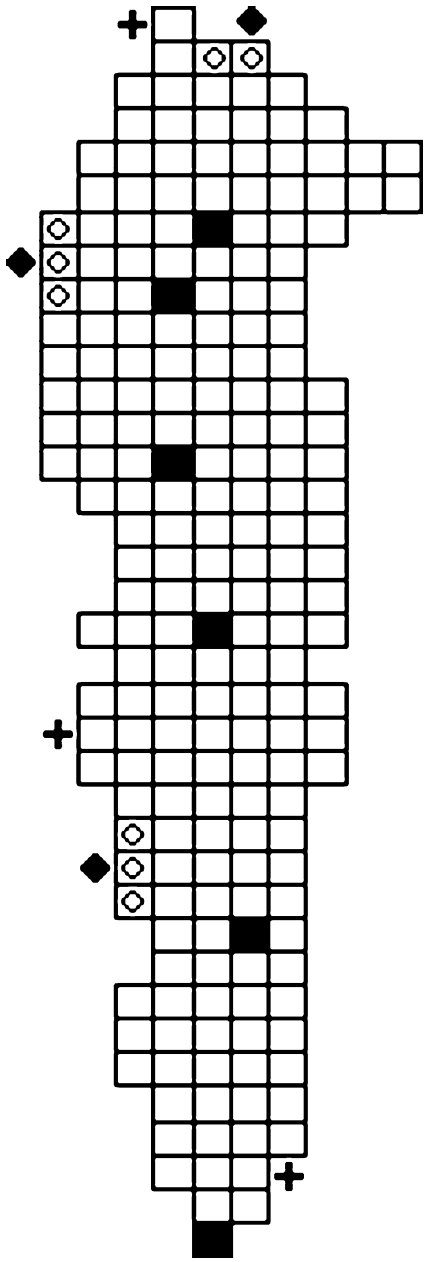

Figure 1. HBEF W6 grid system with 208 25×25 m plots. Black squares are six locations within HBEF W6 where stream NO_3 concentrations were measured by Johnson et al. (2000a). Plus (+) and black diamond (◆) symbols show the locations of weather stations (S9, S10, and S11 in high, middle, and low positions, respectively) and tension free lysimeters outside the HBEF W6 (Johnson et al. 2000a), respectively. The open diamonds (◇) are cells within the HBEF W6 that were used to make comparison with the observed NO_3 concentrations of soil water collected in the tension free lysimeters.

from spatial datasets. SINIC-S was developed as an extension of the aggregated (one-cell) version of the nitrogen cycle model, SINIC (SImple NItrogen Cycle), which reproduced monthly NO_3 export from HBEF W6 during the 1964–1994 period with reasonable accuracy (Hong 2004; Hong et al. 2005). While spatially explicit models are necessary to reproduce the full behavior of spatially extensive systems (Zollweg et al. 1996; Birkinshaw and Ewen 2000), they may also reproduce the average behavior of such systems better than aggregated models (Rupp et al. 2000). We used the SINIC-S model to investigate whether the currently available spatial information at HBEF W6 can explain the elevational pattern in stream NO_3 concentration observed during the 1982–1992 period (Johnson et al. 2000a). We also tested whether the spatially explicit model predicted the streamflow NO_3 flux at the outlet point better than the one-cell model did. Finally, we analyzed the simulation results to identify which watershed processes controlled within-watershed variability of soil N dynamics and NO_3 loss at HBEF W6.

Methods

SINIC-S resulted from our effort to develop a simple model of N cycling for a range of forested watersheds, using conventional descriptions of major N flux processes (Figure 2). These models were constructed within the ECLPSS framework, a generic ecological modeling platform for spatially explicit models (Woodbury et al. 2002). It is currently programmed in MATLAB (http://www.mathworks.com/).

Hydrologic processes

Hydrologic processes considered include daily precipitation/snowpack generation/snowmelt, evapotranspiration, vertical water fluxes between soil layers, interflow, infiltration-excess and saturation-excess runoff, and groundwater flow. Precipitation is assumed to fall as snow when air temperature is below 0 °C. Snowmelt is assumed to occur at a rate proportional to the temperature above freezing (Gray and Prowse 1993), and the proportion of the time in which this occurs is determined by a sinusoidal interpolation between daily max and min temperature. Daily potential evapotranspiration (PET) is calculated using the Penman-Monteith equation (Shuttleworth 1993) adjusted for leaf area index (LAI) using the approach of Federer (1995). PET is partitioned to the various soil layers in proportion to the presence of roots, and estimation of soil moisture-limited evapotranspiration (ET) follows the Thornthwaite-Mather procedure (Steenhuis and Van der Molen 1986). Surface water is lost by evaporation (Rutter et al. 1971). Runoff can be generated from either 'infiltration excess' or 'saturation excess' mechanisms. Infiltration excess runoff is governed by the Soil Conservation Service runoff equation (Rawls et al. 1993). Saturation excess runoff occurs when soil moisture exceeds the saturated value of the entire soil (Zollweg 1994). Infiltration is assumed to be distributed into all soil layers due to the presence of macropores (Federer 1995). Vertical flows redistribute soil water among soil layers. Downward movement of soil water in all soil layers except the bottom layer is based on Darcy's law, assuming gravity flow under unsaturated conditions (Bouraoui et al. 1997). Water draining from the saturated portion of the bottom soil layer is added to the groundwater pool. The daily horizontal interflow flux from a source cell is calculated as the product of the hydraulic conductivity of the soil and the cell slope (Zollweg et al. 1996), applying Darcy's law. An elevation map is used to compute the slope of the cell and the flow proportion to each downhill direction of the eight neighboring cells (Quinn et al. 1991). Once the daily interflow flux from a cell is calculated, it is distributed to each downhill direction according to the flow proportion (Quinn et al. 1995). The groundwater pool is treated as a single aggregate cell for both aggregated and disaggregated models. Groundwater is considered a first-order reservoir in which the baseflow component of daily streamflow is proportional to the residual water in the groundwater pool. Seepage losses to deep aquifers at Hubbard Brook are assumed negligible (Federer 1995).

Nitrogen dynamics processes

Nitrogen dynamics processes include atmospheric input of NH_4^+ and NO_3^- (wet/dry/snowmelt), mineralization of organic N, plant uptake of NH_4^+ and NO_3^-, nitrification, denitrification, ammonia

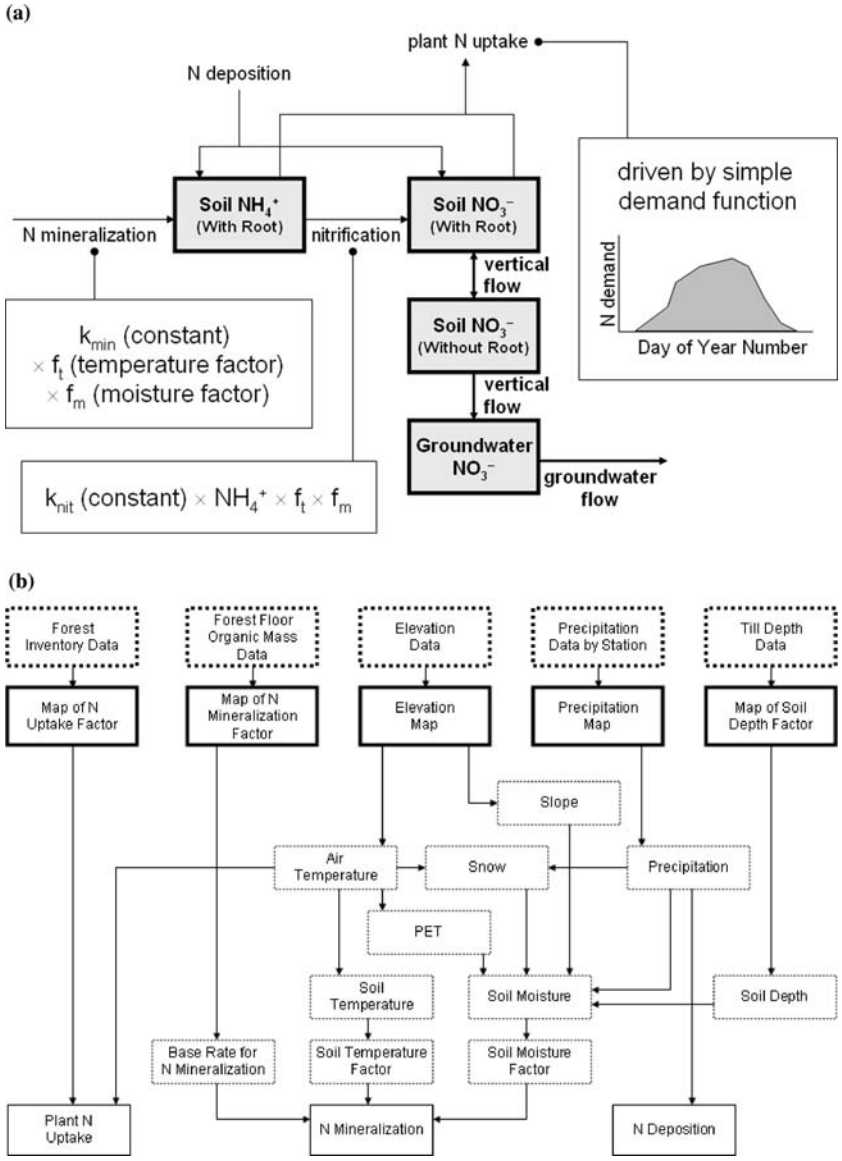

Figure 2. Simplified representation of SINIC model (a) and flow diagram demonstrating how the spatial data are used by SINIC-S to induce the spatial variation in soil N dynamics (b).

volatilization, and interflow and vertical fluxes of NO_3^-/discharge into stream channels. The estimated daily total (wet + dry) N deposition is added to the snowpack when precipitation occurs as snowfall. During snowmelt events, the amount of N released from the snowpack is calculated as snowmelt volume multiplied by the snowpack N concentration. This adjusted daily total N deposition is added to the top soil layer each day of the simulation. N mineralization converts organic N to an input of N to the NH_4^+ pool, governed by microbial activity, in which variations are driven only by soil temperature and moisture. The daily net N mineralization rate is calculated by multiplying two unitless modifying factors as functions of soil temperature (temperature factor) and moisture (moisture factor) by the 'optimum' rate:

$$F_{\min} = k_{\min} \times f_T \times f_M, \quad (1)$$

where $F_{\min}$ = daily net N mineralization rate ($gN/m^2/d$), $k_{\min}$ = daily net N mineralization

rate under 'optimum' condition ($gN/m^2/d$), f_T = temperature factor, f_M = moisture factor. The temperature relationship is based on a modified Q_{10} factor as a function of soil temperature (Johnsson et al. 1987). Soil temperature is modeled as a damped, lagged response to daily average atmospheric temperature (Campbell and Norman 1998). A soil moisture factor is calculated using the moisture content in the soil, determined from the hydrologic component of the model. If the soil moisture is between the saturation and wilting point, there is no restriction in N mineralization by soil moisture. Otherwise, no N mineralization can occur, so the soil moisture factor becomes zero. The daily net N mineralization rate under 'optimum' conditions, assumed to be a fixed value (0.36 $gN/m^2/d$), is obtained from experimental soil incubation studies (Bohlen et al. 2001).

Plant N uptake is calculated as the smaller of two values: the potential plant N demand and the available N in the soil. The potential plant N demand is apportioned throughout the year according to the proportion of growing degree days occurring on each day:

$$D_{\text{day}}(t) = D_{\text{year}} \times \frac{A(t)}{\sum_{i=1}^{365} A(i)}, \qquad (2)$$

where $D_{\text{day}}(t)$ = daily plant N demand on day t ($gN/m^2/d$), D_{year} = annual plant N demand ($gN/m^2/yr$), $A(t)$ = air temperature if air temperature on day t is higher than threshold temperature, otherwise 0. Because the air temperature varies spatially from cell to cell, the shape of demand function varies between cells and from year to year. D_{year} represents the maximum amount of N that can be taken up by plants annually when not limited by soil N availability, but actual plant N uptake is likely to be lower than plant N demand because of limited soil N. Equal affinity for NH_4^+ and NO_3^- is assumed as in PnET-BGC (Gbondo-Tugbawa et al. 2001), so demand is divided into corresponding NH_4^+ and NO_3^- demands according to their relative concentrations. If plant N demand is not satisfied in a cell, and any of the eight neighboring cells have available inorganic nitrogen in the soil, it is assumed that plants can take up nitrogen from them; the remaining demand in the current cell is partitioned in proportion to the available inorganic nitrogen in neighboring cells. The implicit assumption is that N can move either with water or via the local root network from adjacent cells.

Nitrification is simulated as a first-order decay process of soil NH_4^+, with the 'optimum' rate modified by the factors identical to those for N mineralization. The optimum nitrification rate is estimated from soil incubation studies (Vitousek et al. 1982). Denitrification is calculated as in Johnsson et al. (1987). The rate of ammonia volatilization is calculated assuming that (1) ammonia (in gaseous form) is in equilibrium with ammonium (in aqueous form) (Loehr et al. 1973), (2) the ammonia is uniformly distributed through the soil layer, and (3) all of the ammonia in top centimeter of soil is lost each day. A full mathematical description of the model is available in Hong (2004) and also on the web (http://cycas.cornell.edu/ebp/ebpspec/hong_phd/hong_thesis.html).

Generation of gridded maps of driving variables

Gridded maps were created from spatially referenced datasets that characterize the watershed. The five properties affecting the nitrogen cycle which were assumed to vary among cells, and the available datasets providing their spatial distributions are (Figure 3): (1) N mineralization factor, from forest floor organic mass data, (2) N uptake factor, from forest inventory data, (3) precipitation, from multiple weather station data, (4) elevation, from elevation data, and (5) soil depth factor, from till depth data. Each grid cell of the map represents a 25×25 m square plot as delineated on the W6 plot map (Figure 1). Precipitation and elevation maps were used to generate spatially varying meteorological inputs (N deposition, air temperature, PET, etc.) to SINIC-S (Figure 2b). The three dimensionless 'factor' variables permit the time-varying processes developed for a homogeneous model (N mineralization, plant N uptake, etc.) to be distributed spatially over the watershed.

The N mineralization factor was developed on the assumption that spatial variation of N mineralization is driven by spatial variation of forest floor organic matter content. Forest floor organic matter at HBEF W6 (http://www.hubbardbrook.org/yale/forestfloor/) was measured in 1976, 1977,

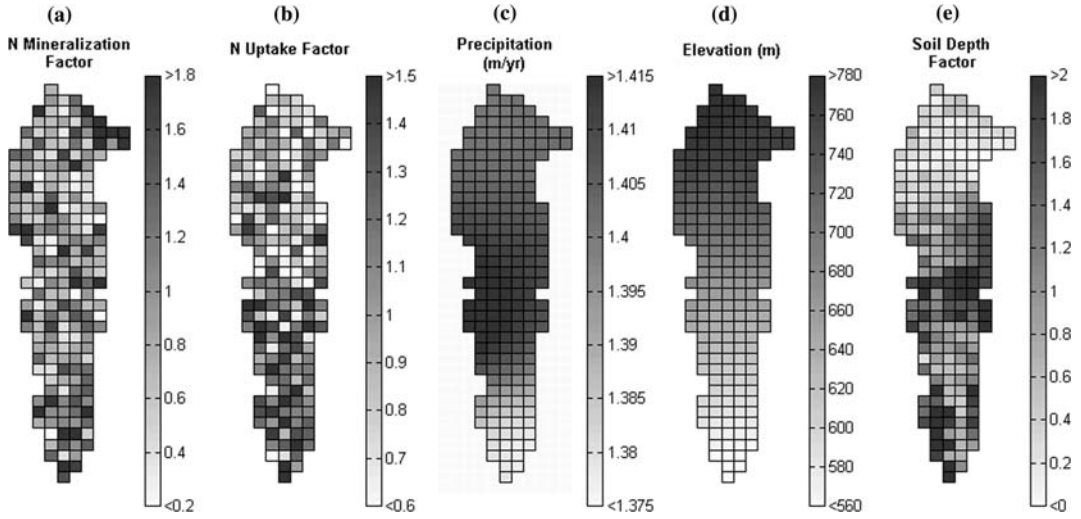

Figure 3. Five gridded maps used by SINIC-S to predict the spatial variation in soil N dynamics and NO_3 loss.

1978, 1982, 1987, 1992, and 1997. A stratified sampling technique was used in which one or more cells were randomly selected from each row. Thus data for all grid cells are not available for each year of measurement. Because only a few measurements were taken in most cells and the observed forest floor organic mass data showed no clear temporal trend, it was assumed that the forest floor organic matter would be best approximated by the average of all measurements taken in each cell. No measurements were taken in seven plots. For these plots, average values of eight neighboring cells were used in place of measurements. The map of the N mineralization factor was generated by dividing the plot values by the average over all plots (Figure 3a). Thus the values in the map are unitless and have an overall mean of 1. To calculate the base rate of N mineralization ($k_{\min}$ in Eq. 1) in each plot during a simulation, map values were multiplied by the watershed average constant base rate estimated from Bohlen et al. (2001). The spatially varying $k_{\min}$ contributed to the spatial pattern in the N mineralization rate (Figure 2b).

The N uptake factor (Figure 3b) was developed on the assumption that the spatial pattern of uptake is determined by the spatial pattern in both the magnitude and rate of change of forest biomass. Forest inventories were conducted at HBEF W6 in 1965, 1977, 1982, 1987, 1992, and 1997 with sampling designs changing over time. Tree biomass was calculated on a plot by plot basis from forest inventory data and available on the web (http://www.hubbardbrook.org/yale/vegetation/). The map of mean biomass was constructed by averaging the plot biomass data over all years. A map of biomass change was constructed by calculating the rate of change in biomass over time (slope in simple linear regression) for each plot. Our calculation of plant N uptake (Hong 2004) suggested that approximately 87% of the estimated plant N uptake is used for leaf and fine root turnover, 7% for wood accumulation, and 6% for herbaceous growth. Following this calculation, we normalized the maps of mean biomass and biomass change by dividing the plot values by their overall plot means (as described in 'N mineralization factor'), and combined them to obtain a gridded map of N uptake factor. Assuming that the spatial variation of leaf and fine root turnover is proportional to that of mean biomass, that spatial variation of wood accumulation is proportional to that of biomass change, and that herbaceous growth is constant over the grid, the mapped value of uptake fraction in each cell was calculated as $0.87\times$ normalized mapped value of mean biomass $+$ $0.07\times$ normalized mapped value of biomass change $+$ 0.06. Again, the values in the map are unitless and the overall mean is 1. During simulation, map values were multiplied by

the constant annual plant N demand (D_{year} in Eq. 2) to calculate D_{year} in each plot. Spatial variation in D_{year} contributed to the spatial pattern in plant N uptake (Figure 2b).

Precipitation has been measured at three weather stations (S9, S10, and S11) near HBEF W6 (http://www.hubbardbrook.org/research/data/atmos/atmos.htm), as shown in Figure 1. Daily precipitation in each cell was interpolated using the inverse-squared-distance weighting method (Fazakas et al. 1999). Because precipitation was measured daily, precipitation maps were constructed for each day of the simulation. The precipitation map in Figure 3c shows the average pattern of precipitation over all simulation days; the daily precipitation maps vary considerably. Spatial variability in N deposition is due solely to the spatial pattern in precipitation; wet N deposition was calculated as the product of precipitation volume and N concentration. N concentration and dry N deposition were assumed to be uniform over the watershed. Spatial variability in precipitation also affected the spatial pattern in N mineralization rate because the soil moisture (hence the soil moisture factor) was affected by precipitation either directly or via snow accumulation in the model (Figure 2b).

Elevations at the four corners of each grid cell (http://www.hubbardbrook.org/yale/mapinfo/w6plotdat.htm) were averaged to construct the map of elevation at the center of each grid cell (Figure 3d). Elevation affected the soil inorganic nitrogen status through several pathways (Figure 2b), primarily through effects on temperature. Lapse rates for air temperature and temperature amplitude (4.5 °C/1000 m and 4.4 °C/1000 m, respectively) were calculated from temperature data collected at two south-facing weather stations outside HBEF W6 (S1 and S6 located at 488 m and 747 m, respectively) and one station adjacent to the Headquarters building at 253 m (http://www.hubbardbrook.org/research/data/wea/wea.htm). Mean air temperature and temperature amplitude for each cell were calculated by adding the product of the lapse rate and elevation of the cell above station S6 to the 'base temperature' measured at station S6. Air temperature in each cell was then used to calculate the corresponding soil temperature and PET, which in turn controlled the soil temperature and moisture factors, respectively. Variations in cell air temperature also affected the spatial pattern of snowmelt, snow accumulation, and plant N uptake (Eq. 2), as well as nitrogen processes affected by temperature variation (e.g. N mineralization and nitrification). Finally, the elevation map was used to calculate cell slopes, which affected the soil moisture pattern via interflow fluxes (Figure 2b).

The soil depth factor follows the pattern of till depth. The HBEF website (http://www.hubbardbrook.org/yale/mapinfo/w6plotdat.htm) indicates that till depth (not soil depth) was measured at HBEF W6 in the late 1960's or early 1970's. We assumed that the spatial distribution of the thickness of soil layers followed the same pattern as that of till depth. The map of soil depth factor was constructed by scaling the plot values by the average over all plots (Figure 3e). The thickness of each soil layer was multiplied by map values to create the spatial variation in soil depth. Soil depth affected the soil moisture (hence the soil moisture factor) by limiting total soil water holding capacity (Figure 2b).

Evaluation methodology

Johnson et al. (2000a) measured stream NO_3 concentrations at six different locations (544, 602, 663, 701, 733, and 751 m) along the elevational gradient of HBEF W6 stream during the 1982–1992 period, and reported the arithmetic (unweighted) averages of stream NO_3 concentrations. The locations of sampling points were identified from Johnson et al. (2000a) and shown in Figure 1. By systematically adding sources of spatial variation in the model, we assessed which of the watershed processes were significant factors in explaining the observed within-watershed variability in stream NO_3 concentration.

To investigate sources of spatial variation, SINIC-S was run with various combinations of five gridded maps described above. When a variable was held constant, its spatial distribution map was replaced with a uniform map of watershed-average values (for example, when the map of N mineralization factor was not used by SINIC-S, the value in each cell was assumed to be 1, which is the average of all 208 cells). For the 'base case' simulation, the spatially explicit model was driven only by spatially uniform values. As spatially varying maps were added to the model, the watershed average base rate of N mineralization (k_{min}) was adjusted to yield the

same mean annual N mineralization rate as the 'base case' simulation, and the annual plant N demand (D_{year}) was adjusted until the simulated mean annual N uptake matched the estimated plant uptake during 1982–1992 period (9.16 gN/m^2/yr).

Average simulated daily stream NO_3 concentrations over the entire simulation period were compared with corresponding observations of the average values of Johnson et al. (2000a) for the six cells shown in Figure 1. Daily concentration was calculated as the daily streamflow NO_3 flux divided by daily streamflow at each location. The daily fluxes at any cell are calculated as the cumulative contribution from all cells up-gradient of the cell. Variation in the elevational pattern of stream NO_3 concentration explained by the model was evaluated using r^2 and normalized mean of squared deviations between measured and predicted concentrations (NMSE = normalized mean square error). The effects of successive addition of spatial variability in input parameters were evaluated by using each of the five gridded maps to individually 'drive' the model, starting from the 'base case' simulation. The simulation resulting in the highest r^2 and the lowest NMSE values was selected. Then each of the remaining four maps was used in addition to the first map to again find the 'best fit' simulation based on the above criteria. This procedure was iterated until all the five maps were added to the model.

Results

Successive addition of spatial variability in model parameters

The model reproduced the observed elevational gradient of stream NO_3 concentration (Johnson et al. 2000a) when N mineralization factor, N uptake factor, elevation, and precipitation all varied spatially throughout the watershed (Table 1 and Figure 4). Of the cases in which spatial variation of only a single variable (i.e. one map) was considered, the N mineralization factor resulted in the highest r^2 value and the lowest NMSE (Table 1). The peak at the 701 m elevation was reproduced when variability of the N uptake factor was considered in addition to that of the N mineralization factor (Figure 4), and 90% of the variation in stream NO_3 concentration was explained by considering variation in both of these factors (Table 1). Additionally incorporating variation in elevation and precipitation shifted the predicted concentrations close to the measured values (Figure 4), reducing the NMSE substantially, but with only a small increase in r^2 (Table 1). The scenario that included variation in all four of these factors yielded the highest r^2 and the lowest NMSE of all possible combinations. When spatial variation in soil depth was incorporated, agreement with the observations decreased markedly (Table 1), resulting in a peak concentration at 663 m (Figure 4).

Table 1. Statistical evaluations of simulated elevational gradients in stream NO_3 concentration.

Map	r^2	NMSE[a]	NME[b]
Nmin	0.72	0.77	−0.16
Uptk	0.00	1.09	0.05
Prcp	0.24	1.05	−0.07
Elev	0.02	1.08	−0.12
Thck	0.18	1.66	0.17
Nmin + Uptk	0.90	0.30	−0.03
Nmin + Uptk + Elev	0.90	0.23	0.02
Nmin + Uptk + Elev + Prcp	0.91	0.22	0.04
Nmin + Uptk + Elev + Prcp + Thck	0.03	1.52	0.27

Data for comparison was obtained from Johnson et al. (2000a). Nmin = map of N mineralization factor; Uptk = map of N uptake factor; Prcp = precipitation map; Elev = elevation map; Thck = map of soil depth factor.

[a]Normalized Mean Square Error = $\Sigma(o_i - p_i)^2/\Sigma(o_i - \bar{o})^2$, where o_i is the ith observation, p_i is the ith prediction, and $\bar{o}$ is the mean of the observations; NMSE = 0 indicates perfect agreement; NMSE = 1 occurs if the mean of the observations is used as the predictor (values of NMSE of one or greater indicate that the modeled values would be better substituted by the mean of the observations).

[b]Normalized Mean Error = bias (mean of differences between the observed and predicted values) divided by mean of observed values; NME = 0 indicates perfect agreement; NME = 1 shows the predictor is biased upward from the observations by 100% on average.

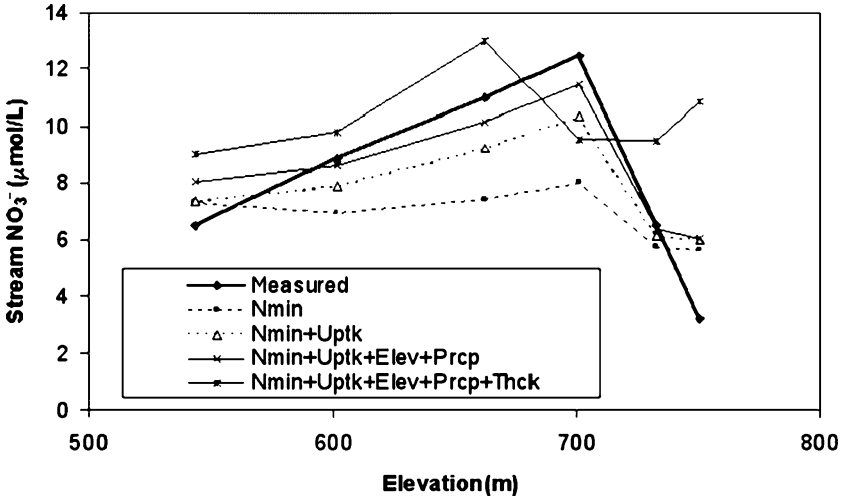

Figure 4. Comparison of elevational gradient in stream NO_3 concentration measured at six locations during the 1982–1992 period within the HBEF W6 (Johnson et al. 2000a) to those simulated with SINIC-S under alternative combinations of spatially distributed driving variables shown in Figure 3. Abbreviations of mapped variable names are explained in Table 1; sample locations are shown in Figure 1.

Model evaluation

Streamflow-weighted average stream NO_3 concentrations were available for the same period at only three locations (544, 663, and 733 m) of the six locations where the measurements of stream NO_3 concentrations were made (C. Johnson, Syracuse University, personal communication). These values were converted into annual streamflow NO_3 fluxes, and compared with the best model predictions obtained above (i.e. considering the spatial variability of N mineralization factor, N uptake factor, elevation, and precipitation). Predicted streamflow NO_3 flux was highest in the middle of the watershed in agreement with the measurements (Figure 5). SINIC-S slightly overpredicted the mean annual streamflow NO_3 flux at 544 and 733 m elevations.

In 1983, zero-tension lysimeters were installed at three different locations outside HBEF W6 (Figure 1), and soil solution chemistry data were collected from these lysimeters at approximately monthly intervals beginning in January 1984 (Johnson et al. 2000a) (http://www.hubbardbrook.

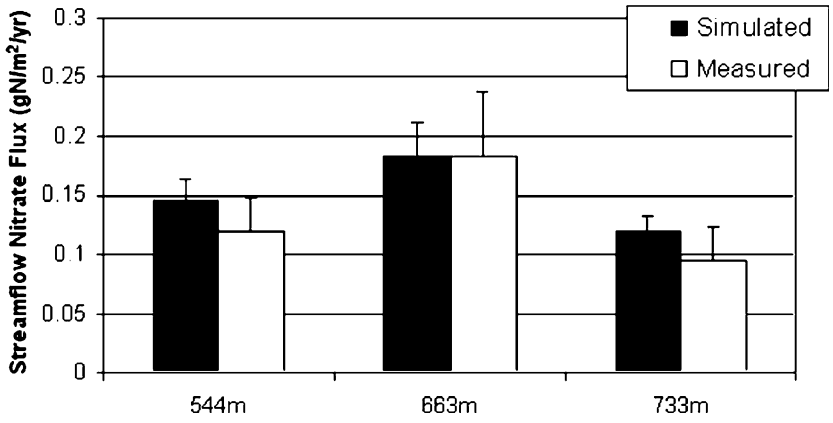

Figure 5. Mean annual streamflow NO_3 flux during the 1982–1992 period at three locations of HBEF W6 stream. Error bars denote + 1 standard errors. Black bar: streamflow NO_3 flux simulated by SINIC-S without the soil thickness map; white bar: measured streamflow NO_3 flux, obtained from C. Johnson (Syracuse University, personal communication).

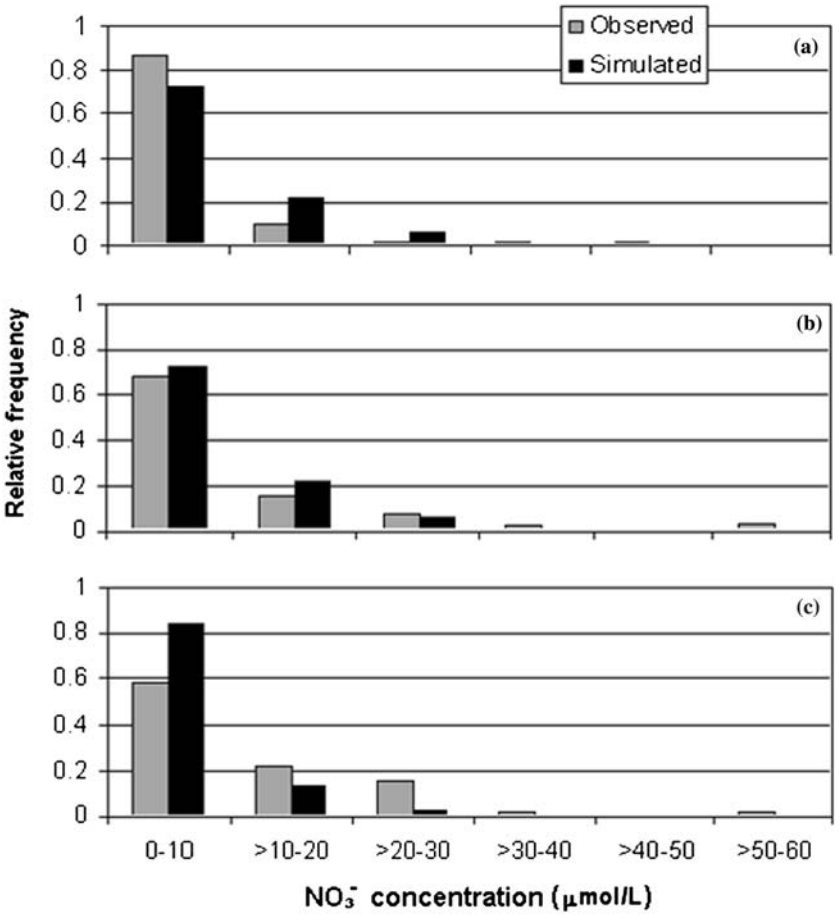

Figure 6. Frequency distributions of observed (gray) and simulated (black) NO_3 concentration (μmol/l) in soil water leached below the rooting zone at three locations outside the HBEF W6 during the 1984–1992 period. The position of the lysimeters (a: high; b: middle; c: low) and the cells used for comparison are shown in Figure 1. Measured concentrations are from soil solution chemistry data in Bs horizon available at HBEF website (http://www.hubbardbrook.org/research/data/soil/lysim/w6lysimdoc.htm). Simulated concentrations are monthly weighted averages of NO_3 concentrations in water lost from cells adjacent to the position of each lysimeter, predicted by SINIC-S without the soil thickness map.

org/research/data/soil/lysim/w6lysimdoc.htm). We compared the frequency distributions of simulated monthly weighted average NO_3 concentration in water lost from the cells adjacent to the position of each lysimeter predicted using all maps except soil depth factor, with frequency distributions of measured NO_3 concentrations in soil water collected in the Bs horizon. Distributions of measured and predicted values at the high elevation (Figure 6a) and middle elevation (Figure 6b) were similar, particularly for concentrations below 10 μmol/l. However, SINIC-S predicted more occurrences of concentrations below 10 μmol/l and fewer occurrences between 20 and 30μmol/l than were measured at the low elevation position (Figure 6c). The model failed to predict some extreme values (30–60 μmol/l) of measured NO_3 concentrations at all locations.

Comparison with aggregated (one-cell) model

The one-cell and the 208-cell versions of the model generated similar predictions of monthly streamflow and streamflow NO_3 flux at the outlet point during the study period (1982–1992). The r^2 value for observed and predicted log-transformed monthly fluxes of streamflow NO_3 increased from 0.58 in the one-cell model (Figure 7a) to 0.63 in the 208-cell model (Figure 7b), suggesting that the

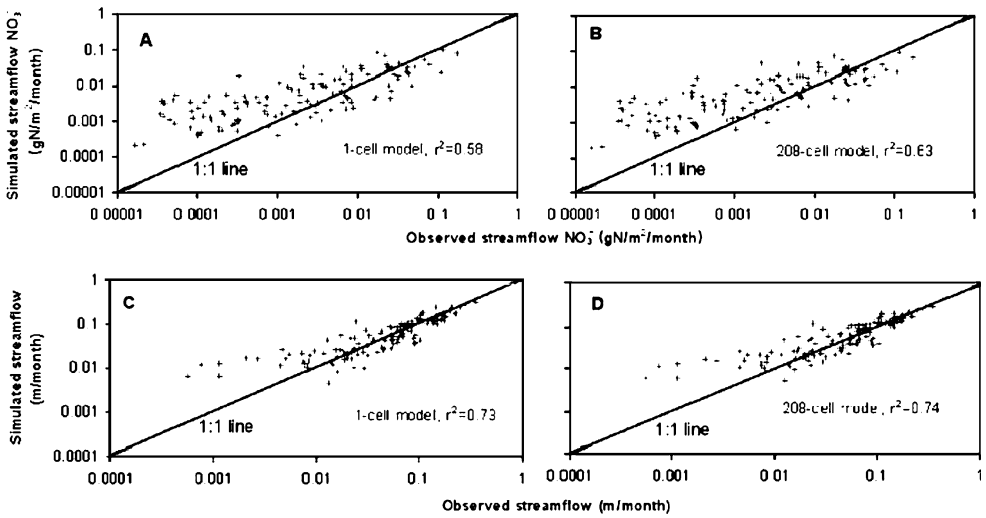

Figure 7. Comparison of measured and simulated monthly streamflow NO_3 loss (a and b) and streamflow (c and d) at the outlet point, expressed on a log scale, during the period of 1982–1992. The fluxes in a and c are simulated with the one-cell version of SINIC, and the fluxes in b and d are simulated with the 208-cell version of SINIC by using all mapped variables in Figure 3 except the soil thickness.

prediction of streamflow NO_3 flux at the outlet point was slightly improved by introducing spatial variability, whereas there was almost no improvement in streamflow prediction (Figures 7c, d). Both models produced estimates of streamflow and streamflow NO_3 flux closer to the 1:1 line when fluxes were relatively high, but there was some upward bias in the model at the low end of the flux distribution.

Spatial variability in soil N dynamics predicted by SINIC-S

The nitrogen pools and fluxes in the 208 cells simulated, using all maps except that of soil depth factor, showed substantial cell-to-cell variation in soil N dynamics and NO_3 loss (Figure 8). Cells with high soil N pools tended to show high fluxes. To understand the spatial interrelationship of soil N dynamics among 208 cells, a correlation matrix was constructed for the simulated mean annual values of variables over the 1982–1992 periods in each of the 208 cells (Table 2). Mean annual NO_3 loss was highly correlated in space with the difference between the mean annual rates of N mineralization and N uptake, as well as with nitrification rate, soil NO_3^-, and soil NH_4^+. Mineralization and uptake, highly correlated in space, were not highly correlated with NO_3 loss when considered individually (though the correlations were statistically different from 0). N deposition was not highly correlated with any of the variables.

Discussion

Using gridded maps to simulate spatial variability in soil N dynamics

Our simulation results suggest that available information on spatial heterogeneity in biotic, topographic, and climatic variables within HBEF W6 is sufficient to reproduce much of the observed elevational pattern in stream NO_3 concentration. By using the gridded maps of selected driving variables as spatially varying input parameters, as much as 91% of the variation in stream NO_3 concentration during the period 1982–1992 was explained by SINIC-S (Table 1), demonstrating that the spatial datasets collected within the HBEF W6 can be used to characterize the spatial variability of model parameters that govern the soil N dynamics and NO_3 loss (N mineralization, N uptake, and N deposition; Figure 2b).

While it has become a conventional practice in ecological and biogeochemical modeling to

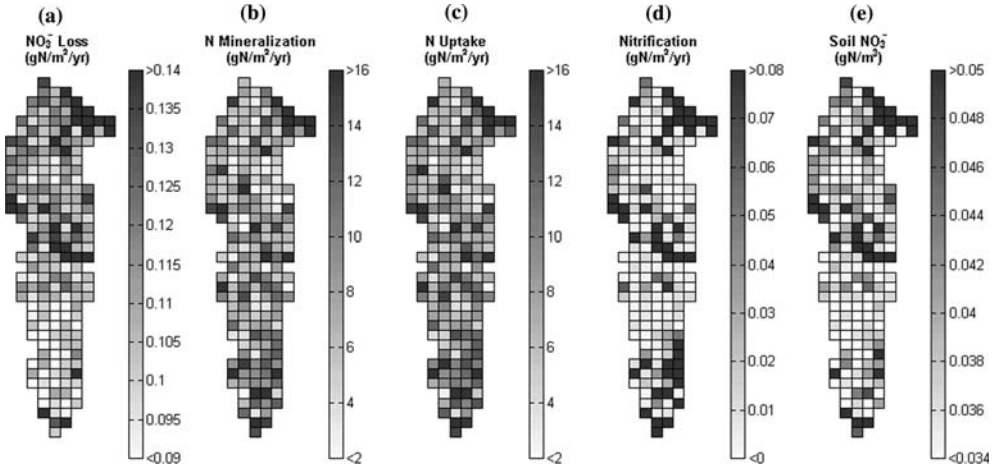

Figure 8. Spatial variation in nitrogen pools and fluxes simulated by SINIC-S without the soil thickness map during the 1982–1992 period.

Table 2. Spatial correlations between SINIC-S variables over the 208 grid cells.

Variable	X_1	X_2	X_3	X_4	X_5	X_6	X_7	X_8
X_1	–	0.403*	0.383*	0.006	0.700*	0.979*	0.879*	0.820*
X_2	–	–	0.999*	−0.183*	0.811*	0.467*	0.744*	0.552*
X_3	–	–	–	−0.186*	0.811*	0.452*	0.737*	0.544*
X_4	–	–	–	–	−0.233*	−0.088	−0.160*	−0.177*
X_5	–	–	–	–	–	0.769*	0.928*	0.809*
X_6	–	–	–	–	–	–	0.929*	0.816*
X_7	–	–	–	–	–	–	–	0.836*
X_8	–	–	–	–	–	–	–	–

The log-transformed annual values over the 1982–1992 periods simulated in each of the 208 cells were used. Correlations significant at the 95% confidence level are indicated by *. X_1 = NO_3 loss; X_2 = N mineralization; X_3 = N uptake; X_4 = N deposition; X_5 = nitrification; X_6 = soil NO_3; X_7 = soil NH_4^+; X_8 = N mineralization – N uptake.

discretize a landscape into grid cells, construct maps of variables from available data, and use the maps as spatially varying input parameters of a multi-cell model (Kuo et al. 1999; Jenkins et al. 1999), large uncertainties exist in the map construction process. In most cases not enough data exist to develop maps for all input parameters of the model (Abbott et al. 1986). The SINIC model has approximately 40 input parameters (Hong 2004), all of which may vary spatially within HBEF W6. Although these parameters have physical meanings and can be estimated from field data, it is impractical to measure them directly in every grid cell. We were able to use available spatial information to estimate the spatial variation of a few selected parameters that were expected to play a key role in spatial dynamics. For example, because this watershed has a relatively homogeneous species composition, we assumed that spatial variation of the base rate for N mineralization (k_{min} in Eq. 1) is driven by spatial variation of forest floor organic matter content. Although the forest floor organic matter content reflects the pool size of potentially mineralizable organic matter and is a major determinant of microbial biomass and soil N cycling rates (Bohlen et al. 2001), other factors such as C:N ratio (Ollinger et al. 2002), lignin and nutrient concentrations (Berg 2000), and species composition (Verchot et al. 2001), also control k_{min} values. The overprediction of stream NO_3 concentration at the highest sampling location (Figure 4) suggests that the net N mineralization rate at this location may have been overestimated by the absence of a specific estimate of the lower litter quality under the spruce-fir stands (Lawrence et al. 2000; Venterea

et al. 2003). Uncertainties in the map construction process may also arise because different ecosystem properties have different scales of spatial heterogeneity (Litaor et al. 2002). Although the spatial information was presented at the 25×25 m plot scale in this study, some soil properties may vary at spatial scales < 1 m (Johnson et al. 2000b).

Evaluation of successive addition of spatially varying maps

Spatial variability of a system can be predicted more accurately as additional spatial information is provided to the spatially explicit model (Mackay 2001). In this study, successive additions of the maps of N mineralization factor, N uptake factor, elevation, and precipitation enhanced the r^2 values to 0.72, 0.90, 0.90, and 0.91, and reduced NMSE to 0.77, 0.30, 0.23, and 0.22, respectively (Table 1). Model performance improved substantially with the successive addition of the first two sources of variability, while the addition of the last two sources added little to the model prediction of elevational pattern in stream N concentration. In this small watershed, spatial variation in biotic factors (potential N mineralization and plant N demand) played a more important role in the spatial pattern of soil N dynamics and streamflow NO_3 flux than did climatic (precipitation) and topographic (elevation) factors, in part because of the greater spatial variation of biotic factors compared to the abiotic factors (Figure 3). Studies by Johnson et al. (2000a) and Lovett et al. (1996) suggest that the precipitation and N deposition probably do not show a large spatial variation within the Hubbard Brook region. Litaor et al. (2002) and Johnson et al. (2000b) reported that spatial variation in topographic factors could not explain the spatial variations in soil processes, which occurred at much finer scales. Although biotic factors are not independent of climatic and topographic factors (Frelich et al. 1993), our simulation results suggest that better estimation of spatial variation of biotic factors may improve predictions of the spatial pattern of soil N dynamics and streamflow NO_3 flux.

Adding spatial information to the model did not always lead to better agreement with observations. We expected that incorporating spatial variability of soil depth might further improve model predictions by reducing the overpredictions at the highest and the lowest elevations (Figure 4). Thinner soil in the upper watershed (Figure 3e) has lower water holding capacity (Bohlen et al. 2001), which could have led to a dryer soil and lower net N mineralization rates, while thicker soil in the lower watershed may increase the nutrient-water contact time (Johnson et al. 2000a), possibly increasing the rate of NO_3 loss by denitrification. Instead of an improvement, however, the pattern of predicted stream NO_3 concentration, including position of peak concentration, deviated from observations when spatial variation in the soil depth factor was added to the model (Figure 4), resulting in an r^2 value close to 0 and NMSE > 1 (Table 1). Among the possible reasons for deviations between these predictions and observations are: (1) till depth was estimated in the late 1960's or early 1970's using a device of uncertain accuracy (http://www.hubbardbrook.org/yale/mapinfo/w6plotdat.htm), (2) although they show similar spatial patterns (Johnson et al. 2000a), spatial variation in till depth may not be a good indicator of that of soil depth, and (3) the SINIC-S algorithms handling the variation in soil depth may be biased. Although the use of a soil map having soil thickness information is a desirable way of creating the map of soil depth factor, spatially distributed soil profile data for HBEF W6 at the level of resolution required to do so for our model are nonexistent, to the best of our knowledge. In light of this, we chose to use a relatively simple approach based on available data (i.e., till depth), which essentially assumes that spatial variation in layer thickness is relatively low, and thus the hydraulic gradient between cells can be approximated by elevational differences. This approach has been used successfully by other studies (e.g., Zollweg et al. 1996; Bronstert 1999) and given the relatively small relative magnitude of interflow in this case (Hong 2004), we believe this approximation to be adequate.

A spatial model can be evaluated using multiple criteria (Guntner et al. 1999; Band et al. 2001), and it is generally much more difficult to predict point measurements rather than integrative measures (Johnson et al. 2000b). Although SINIC-S predicted integrative measures such as stream NO_3

concentration (Figure 4) and streamflow NO_3 flux (Figure 5) reasonably well, soil solution chemistry predicted at three different positions of HBEF W6 deviated from observations, especially at the lowest position (Figure 6c). Considering that the predicted soil NO_3 concentration exhibited a substantial variation among 208 cells (Figure 8e), and that observations of soil solution chemistry were made outside the watershed (Johnson et al. 2000a), it is possible that the comparison was not made in the 'correct' positions, although the cells closest to the measurement points were selected for comparison (Figure 1).

The spatial model can also be evaluated by comparison with an aggregated (one-cell) model. Consideration of spatial variability of the system generally should lead to better prediction of overall behavior (Beasley et al. 1982). However, Rupp et al. (2000) reported that a spatial model produced exactly the same results as the aggregated model in some cases, and better results in other cases, and that it was difficult to determine conditions under which a spatial model will be superior to an aggregated version of the model. In our study, the aggregated model and the spatially explicit model produced almost identical results for outflows, with the spatial model predictions showing a slightly better r^2 for streamflow NO_3 flux (Figures 7a, b), but not for streamflow (Figures 7c, d). Although the water and nitrate are routed from cell to cell to the outlet of the watershed through the interflow fluxes, vertical fluxes adding water and NO_3 to the groundwater pool (which is represented as an aggregated cell even in the spatially explicit model) were the dominant contributions to the streamflow and streamflow NO_3 flux in this small and steep watershed. This lack of cell-to-cell interaction may be the reason for the similar behavior between two models.

Factors controlling spatial variation in soil N dynamics and nitrate loss

SINIC-S exhibited substantial cell-to-cell variations in soil N dynamics and NO_3 loss within the HBEF W6 during the simulation period (Figure 8). The analysis of simulation results suggested that the spatial pattern of NO_3 loss within the watershed was driven by the interaction of N mineralization and plant N uptake, for the following reasons. First, as discussed above, the combination of the spatial distribution of N mineralization factor and that of N uptake factor, but not the individual factors alone, explained most of the elevational pattern in stream NO_3 concentration (Table 1 and Figure 4). Second, the spatial correlation matrix for simulated mean annual values over the simulation period (Table 2) revealed that the cell NO_3 loss was highly correlated with the difference between N mineralization and N uptake over the 208 grid cells. The individual variables were also significantly correlated with NO_3 loss, but their correlation coefficients were much lower than the coefficient of their difference (Table 2). Third, the investigation of N dynamics in the sub-basins of the watershed along the six sampling points of the elevational gradient, calculated by subtracting the cumulative values at the next higher position from the cumulative values at the current position, revealed that the difference between N mineralization and N uptake showed the same elevational pattern as the pattern of simulated streamflow NO_3 flux (Figure 9). Neither N mineralization nor N uptake, when considered individually, followed the elevational pattern of NO_3 loss.

It has been well demonstrated that the elevational pattern in stream NO_3 concentration at HBEF is tightly linked to that in soil inorganic N pool (Bohlen et al. 2001). How elevation controls the soil NO_3 content, however, is still a challenging question, partly because elevation, either directly or indirectly, affects many driving variables such as temperature (Lawrence et al. 2000), deposition (Weathers et al. 2000), forest biomass (Johnson et al. 2000a), and soil organic matter (Bohlen et al. 2001), which together control the soil NO_3 content. None of the driving variables used in this study (Figure 3) showed the same elevational pattern as the simulated stream NO_3 concentration, and it was necessary to consider the elevational pattern of more than one driving variable. For example, simulated N mineralization was actually highest at the lowest elevation due to higher forest floor organic matter content (Figure 9). Adding spatial variation of N uptake factor (Figure 3b) to the model increased simulated N uptake in the lower part of the watershed, so that while mineralized inorganic N was higher at the lowest elevation, available N was

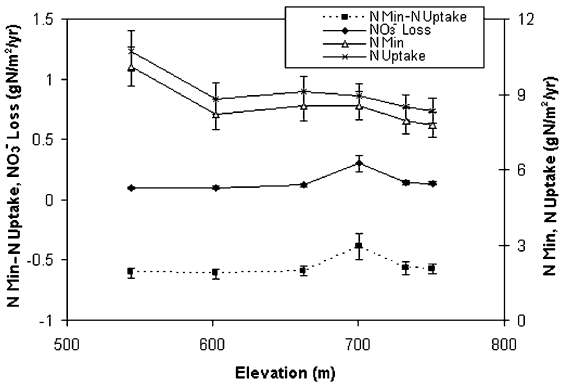

Figure 9. The elevational pattern of simulated N mineralization, N uptake, and their difference, as well as mean annual NO_3 loss simulated in six sub-basins of the HBEF W6 during the 1982–1992 period. Error bars denote ± 1 standard errors.

effectively taken up by the plants (Figure 9). This explanation is consistent with the conclusion by Johnson et al. (2000a) that net biomass accumulation, which occurred only in the lower part of the watershed during the simulation period (probably due to higher temperature at lower elevation), was in part responsible for the higher retention of NO_3 at the low elevation area and the declining pattern of stream NO_3 concentration. Based on these analyses, we conclude that the spatial pattern in the difference between N mineralization and N uptake, but not the individual factors, drives the spatial pattern in the NO_3 loss at HBEF W6 during the simulation period. Because the map of N mineralization factor (created from forest floor organic mass data) and the map of N uptake factor (created from forest inventory data) drive the spatial patterns of N mineralization and N uptake, respectively, we conclude that the spatial distributions of forest floor organic mass and standing biomass are most responsible for creating the elevational pattern in stream NO_3 concentration within the HBEF W6.

In a previous study using the aggregated model, Hong et al. demonstrated that temporal variation in streamflow NO_3 flux was driven mainly by temporal variation in climatic variables (air temperature and precipitation) determining the soil temperature and moisture factors (Hong 2004; Hong et al. 2005). However, factors controlling the spatial variation in soil N dynamics and NO_3 loss are not expected to be the same as those controlling the temporal pattern. While temporal variation in temperature and moisture factors from year to year is much greater than their spatial variation in this small (13.2 ha) watershed, the cell-to-cell variation in biotic factors (e.g. plant biomass and forest floor organic matter content) is much greater than their interannual variation, and spatial patterns of NO_3 flux are thus more dependent on them.

We believe that the elevational pattern of stream NO_3 concentration in relatively small forested watersheds can be explained by taking a similar approach to that presented in this study, and we are envisioning the application of our approach to a number of watersheds in the northeastern US, such as sub-basins of the Catskill Mountains that have shown elevational variation in stream NO_3 concentration (Lawrence et al. 2000). We emphasize that our present analysis should be interpreted and applied at the spatial scale of W6 only, which is relatively small and homogeneous. The spatial pattern identified depends on the scale of the study (Oline and Grant 2002), and watershed-level studies are often highly sensitive to the spatial scale (Johnson et al. 2000a). As watershed size increases, the relative importance of variation in individual cells decreases, and stream chemistry in forested watersheds generally stabilizes after a certain size in spite of increasing variation in bedrock type and species composition (Wolock et al. 1997; Johnson et al. 2000a). The overall heterogeneity of driving variables also generally increase with increasing scale, and if the same analysis were performed on a large watershed with widely varying topography (Weathers et al. 2000) or land use types (Kuusemets and Mander 2002), across watersheds (Kortelainen et al. 1997; Lovett et al. 2000), or over the timescale of centuries where significant changes in plant and soil organic matter pools are expected (Parton et al. 1983), different conclusions may be obtained. In spite of these possible limitations, we believe that our study presents a valuable insight into how the elevational pattern in stream chemistry in small forested watersheds is influenced by spatial distribution of biotic, climatic, and topographic factors.

Acknowledgements

This research was funded by the United States Environmental Protection Agency (EPA) High

Performance Computing program, grant number: R 825208-01-0. Additional support was provided by an educational support grant to Boyce Thompson Institute from the Alcoa Foundation and the National Science Foundation (DEB-0238121). The sponsors of this research have not formally reviewed this document and it should not be construed to represent their policies. Some data used in this publication was obtained by scientists of the Hubbard Brook Ecosystem Study; this publication has not been reviewed by those scientists. The precipitation and streamwater chemistry data were provided by Gene E. Likens through funding by the National Science Foundation and the A.W. Mellon Foundation. The Hubbard Brook Experimental Forest is operated and maintained by the Northeastern Research Station, U.S. Department of Agriculture, Newtown Square, Pennsylvania. We thank Dr Chris Johnson for sharing data on stream NO_3 concentration, Dr Karin Limburg and Dr Timothy Fahey for reviewing an early draft of the manuscript and Dr Peter Woodbury for his collaboration in work leading up to this research.

References

Abbott M.B., Bathurst J.C., Cunge J.A., O'Connell P.E. and Rasmussen J. 1986. An introduction to the European hydrological system-Systeme Hydrologique Europeen, SHE, 1. History and philosophy of a physically-based, distributed modeling system. J. Hydrol. 87: 45–59.

Band L.E., Tague C.L., Groffman P. and Belt K. 2001. Forest ecosystem processes at the watershed scale: hydrological and ecological controls of nitrogen export. Hydrol. Process. 15: 2013–2028.

Beasley D.B., Huggins L.F. and Monke E.J. 1982. Modeling sediment yields from agricultural watersheds. J. Soil Water Conserv. 37: 113–117.

Berg B. 2000. Initial rates and limit values for decomposition of Scots pine and Norway spruce needle litter: a synthesis for N-fertilized forest stands. Can. J. For. Res. 30: 122–135.

Bernhardt E.S., Hall R.O. and Likens G.E. 2002. Whole-system estimates of nitrification and nitrate uptake in streams of the Hubbard Brook Experimental Forest. Ecosystems 5: 419–430.

Birkinshaw S.J. and Ewen J. 2000. Modelling nitrate transport in the Slapton Wood catchment using SHETRAN. J. Hydrol. 230: 18–33.

Bohlen P.J., Groffman P.M., Driscoll C.T., Fahey T.J. and Siccama T.G. 2001. Plant–soil-microbial interactions in a northern hardwood forest. Ecology 82: 965–978.

Bouraoui F., Vachaud G., Haverkamp R. and Normand B. 1997. A distributed physical approach for surface-subsurface water transport modeling in agricultural watersheds. J. Hydrol. 203: 79–92.

Brierley E.D.R., Shaw P.J.A. and Wood M. 2001. Nitrogen cycling and proton fluxes in an acid forest soil. Plant Soil 229: 83–96.

Bronstert A. 1999. Capabilities and limitations of detailed hillslope hydrological modelling. Hydrol. Process. 13: 21–48.

Campbell G.S. and Norman J.M. 1998. An Introduction to Environmental Biophysics, 2nd ed. Springer-Verlag, New York, USA.

Christ M.J., Peterjohn W.T., Cumming J.R. and Adams M.B. 2002. Nitrification potentials and landscape, soil and vegetation characteristics in two Central Appalachian watersheds differing in NO_3^- export. Forest Ecol. Manage. 159: 145–158.

Clay D.E., Carlson C.G., Brix-Davis K., Oolman J. and Berg B. 1997. Soil sampling strategies for estimating residual nitrogen. J. Product. Agricult. 10: 446–452.

Fazakas Z., Nilsson M. and Olsson H. 1999. Regional forest biomass and wood volume estimation using satellite data and ancillary data. Agricult. Forest Meteorol. 98(99): 417–425.

Federer C.A. 1995. BROOK90: a simulation model for evaporation, soil water, and streamflow. General Technical Report NE-141. USDA Forest Service, Durham, New Hampshire, USA.

Frelich L.E., Calcote R.R., Davis M.B. and Pastor J. 1993. Patch formation and maintenance in an old-growth hemlock-hardwood forest. Ecology 74: 513–527.

Gbondo-Tugbawa S.S., Driscoll C.T., Aber J.D. and Likens G.E. 2001. Evaluation of an integrated biogeochemical model (PnET-BGC) at a northern hardwood forest ecosystem. Water Resour. Res. 37: 1057–1070.

Gray D.M. and Prowse T.D. 1993. Snow and floating ice. In: Maidment D.R. (ed.), Handbook of Hydrology. McGraw-Hill, New York, USA, pp. 7.1–7.58.

Guntner A., Uhlenbrook S., Seibert J. and Leibundgut C. 1999. Multi-criterial validation of TOPMODEL in a mountainous catchment. Hydrol. Process. 13: 1603–1620.

Hall R.O., Bernhardt E.S. and Likens G.E. 2002. Relating nutrient uptake with transient storage in forested mountain streams. Limnol. Oceanogr. 47: 255–265.

Hinkle S.R., Duff J.H., Triska F.J., Laenen A., Gates E.B., Bencala K.E., Wentz D.A. and Silva S.R. 2001. Linking hyporheic flow and nitrogen cycling near the Willamette River – a large river in Oregon, USA. J. Hydrol. 244: 157–180.

Hong B. 2004. Controls on the temporal and spatial patterns of streamflow nitrate flux at Hubbard Brook Watershed Six, New Hampshire, USA. Ph.D. Thesis, Cornell University, Ithaca, New York, USA, 306 pp.

Hong B., Swaney D.P., Woodbury P.B. and Weinstein D.A. 2005. Long-term nitrate export pattern from Hubbard Brook Watershed 6 driven by climatic variation. Water Air Soil Pollut. 160: 293–326.

Jenkins J.C., Kicklighter D.W., Ollinger S.V., Aber J.D. and Melillo J.M. 1999. Sources of variability in net primary production predictions at a regional scale: a comparison using PnET-II and TEM 4.0 in northeastern US forests. Ecosystems 2: 555–570.

Johnson C.E., Driscoll C.T., Siccama T.G. and Likens G.E. 2000a. Element fluxes and landscape position in a northern hardwood forest watershed ecosystem. Ecosystems 3: 159–184.

Johnson C.E., Ruiz-Mendez J.J. and Lawrence G.B. 2000b. Forest soil chemistry and terrain attributes in a Catskills watershed. Soil Sci. Soc. Am. J. 64: 1804–1814.

Johnsson H., Bergstrom L., Jansson P.E. and Paustian K. 1987. Simulated nitrogen dynamics and losses in a layered agricultural soil. Agricult. Ecosyst. Environ. 18: 333–356.

Kortelainen P., Saukkonen S. and Mattsson T. 1997. Leaching of nitrogen from forested catchments in Finland. Global Biogeochem. Cycles 11: 627–638.

Kuo W.L., Steenhuis T.S., McCulloch C.E., Mohler C.L., Weinstein D.A., DeGloria S.D. and Swaney D.P. 1999. Effect of grid size on runoff and soil moisture for a variable-source-area hydrology model. Water Resour. Res. 35: 3419–3428.

Kuusemets V. and Mander Ü. 2002. Nutrient flows and management of a small watershed. Landscape Ecol. 17(Supplement 1): 59–68.

Laverman A.M., Zoomer H.R., Van Verseveld H.W. and Verhoef H.A. 2000. Temporal and spatial variation of nitrogen transformations in a coniferous forest soil. Soil Biol. Biochem. 32: 1661–1670.

Lawrence G.B., Lovett G.M. and Baevsky Y.H. 2000. Atmospheric deposition and watershed nitrogen export along an elevational gradient in the Catskill Mountains, New York. Biogeochemistry 50: 21–43.

Litaor M.I., Seastedt T.R. and Walker D.A. 2002. Spatial analysis of selected soil attributes across an alpine topographic/snow gradient. Landscape Ecol. 17: 71–85.

Loehr R.C., Prakasam T.B.S., Srinath E.G. and Joo Y.D. 1973. Development and demonstration of nutrient removal from animal wastes. EPA Series Report R2–73–095. USEPA, Washington D.C., USA, 340 pp.

Lovett G.M., Weathers K.C. and Sobczak W.V. 2000. Nitrogen saturation and retention in forested watersheds of the Catskill Mountains, New York. Ecol. Appl. 10: 73–84.

Lovett G.M., Nolan S.S., Driscoll C.T. and Fahey T.J. 1996. Factors regulating throughfall flux in a new New-Hampshire forested landscape. Can. J. Forest Res. 26: 2134–2144.

Mackay D.S. 2001. Evaluation of hydrologic equilibrium in a mountainous watershed: incorporating forest canopy spatial adjustment to soil biogeochemical processes. Adv. Water Resour. 24: 1211–1227.

Manderscheid B. and Matzner E. 1995. Spatial heterogeneity of soil solution chemistry in a mature Norway spruce (*Picea abies* (L.) Karst.) stand. Water Air Soil Pollut. 85: 1185–1190.

Oline D. and Grant M. 2002. Scaling patterns of biomass and soil properties: an empirical analysis. Landscape Ecol. 17: 13–26.

Ollinger S.V., Smith M.L., Martin M.E., Hallett R.A., Goodale C.L. and Aber J.D. 2002. Regional variation in foliar chemistry and N cycling among forests of diverse history and composition. Ecology 83: 339–355.

Parton W.J., Anderson D.W., Cole C.V. and Stewart J.W.B. 1983. Simulation of soil organic matter formations and mineralization in semiarid agroecosystems. In: Lowrance R., Todd R., Asmussen L. and Leonard R. (eds), Nutrient Cycling in Agricultural Ecosystems. University of Georgia Press, Athens, Georgia, USA, pp. 533–550.

Quinn P., Beven F. and Lamb R. 1995. The $(\alpha/\tan\beta)$ index: how to calculate it and how to use it within the TOPMODEL framework. Hydrolog. Process. 9: 161–182.

Quinn P., Beven K., Chevallier P. and Planchon O. 1991. The prediction of hillslope flow paths for distributed hydrological modeling using digital terrain models. Hydrol. Process. 5: 59–80.

Rawls W.J., Ahuja L.R., Brakensiek D.L. and Shirmohammadi A. 1993. Infiltration and soil water movement. In: Maidment D.R. (ed.), Handbook of Hydrology. McGraw-Hill, New York, USA, pp. 5.1–5.51.

Rupp T.S., Starfield A.M. and Chapin F.S.III 2000. A frame-based spatially explicit model of subarctic vegetation response to climate change: comparison with a point model. Landscape Ecol. 15: 383–400.

Rutter A.J., Kershaw K.A., Robins P.C. and Morton A.J. 1971. A predictive model of rainfall interception in forests, 1. Derivation of the model from observations in a plantation of Corsican pine. Agricult. Meteorol. 9: 367–384.

Shuttleworth W.J. 1993. Evaporation. In: Maidment D.R. (ed.), Handbook of Hydrology. McGraw-Hill, New York, USA, pp. 4.1–4.53.

Steenhuis T.S. and der Molen W.H. 1986. The Thornthwaite-Mather procedure as a simple engineering method to predict recharge. J. Hydrol. 84: 221–229.

Venterea R.T., Lovett G.L., Groffman P.M. and Schwarz P.A. 2003. Landscape patterns of net nitrification in a northern hardwood-conifer forest. Soil Sci. Soc. Am. J. 67: 527–539.

Verchot L.V., Holmes Z., Mulon L., Groffman P.M. and Lovett G.M. 2001. Gross vs net rates of N mineralization and nitrification as indicators of functional differences between forest types. Soil Biol. Biochem. 33: 1889–1901.

Vitousek P.M., Gosz J.R., Grier C.C., Melillo J.M. and Reiners W.A. 1982. A comparative-analysis of potential nitrification and nitrate mobility in forest ecosystems. Ecol. Monogr. 52: 155–177.

Weathers K.C., Lovett G.M., Likens G.E. and Lathrop R. 2000. The effect of landscape features on deposition to Hunter Mountain, Catskill Mountains, New York. Ecol. Appl. 10: 528–540.

Wickham J.D., Wade T.G., Riitters K.H., O'Neill R.V., Smith J.H., Smith E.R., Jones K.B. and Neale A.C. 2003. Upstream-to-downstream changes in nutrient export risk. Landscape Ecol. 18(2): 195–208.

Williard K.W.J., DeWalle D.R., Edwards P.J. and Schnabel R.R. 1997. Indicators of nitrate export from forested watersheds of the mid-Appalachians, United States of America. Global Biogeochem. Cycles 11: 649–656.

Wolock D.M., Fan J. and Lawrence G.B. 1997. Effects of basin size on low-flow stream chemistry and subsurface contact time in the Neversink River watershed, New York. Hydrol. Process. 11: 1273–1286.

Woodbury P.B., Beloin R.M., Swaney D.P., Gollands B.E. and Weinstein D.A. 2002. Using the ECLPSS software environment to build a spatially explicit component-based model of ozone effects on forest ecosystems. Ecol. Model. 150: 211–238.

Zollweg J.A., Gburek W.J. and Steenhuis T.S. 1996. SMoR-Mod-a GIS-integrated rainfall-runoff model. Trans. ASAE 39: 1299–1307.

Zollweg J.A. 1994. Effective use of geographic information systems for rainfall-runoff modeling. Ph.D. Thesis, Cornell University, Ithaca, New York, USA, 172 pp.